HHS Public Access

Author manuscript

Invest Radiol. Author manuscript; available in PMC 2018 October 01.

Published in final edited form as:

Invest Radiol. 2017 October ; 52(10): 583–589. doi:10.1097/RLI.0000000000000375.

Comprehensive dynamic contrast-enhanced 3D MR imaging of the breast with fat/water separation and high spatiotemporal resolution using radial sampling, compressed sensing, and parallel imaging

Thomas Benkert, PhD[1,2], **Kai Tobias Block, PhD**[1,2], **Samantha Heller, MD**[1,2], **Melanie Moccaldi**[1,2], **Daniel K Sodickson, PhD, MD**[1,2], **Sungheon Gene Kim, PhD**[1,2], and **Linda Moy, MD**[1,2]

[1]Center for Advanced Imaging Innovation and Research (CAI[2]R), Department of Radiology, New York University School of Medicine, New York, NY USA

[2]Bernard and Irene Schwartz Center for Biomedical Imaging, Department of Radiology, New York University School of Medicine, New York, NY USA

Abstract

Objectives—To assess the applicability of Dixon RAdial Volumetric Encoding (Dixon-RAVE) for comprehensive dynamic contrast-enhanced 3D MR imaging of the breast using a combination of radial sampling, model-based fat/water separation, compressed sensing, and parallel imaging.

Materials and Methods—In this Health Insurance Portability and Accountability Act (HIPAA)-compliant prospective study, 24 consecutive patients underwent bilateral breast MRI, including both conventional fat-suppressed and non-fat-suppressed pre-contrast T1-weighted Volumetric Interpolated Breath-hold Examination (VIBE). Afterwards, one continuous Dixon-RAVE scan was performed with the proposed approach while the contrast agent was injected. This scan was immediately followed by the acquisition of four conventional fat-saturated VIBE scans. From the comprehensive Dixon-RAVE dataset, different image contrasts were reconstructed that are comparable to the separate conventional VIBE scans.

Two radiologists independently rated image quality (IQ), conspicuity of fibroglandular tissue from fat (FG), and degree of fat suppression (FS) on a 5-point Likert-type scale for the following three comparisons: pre-contrast fat-suppressed (pre-FS), pre-contrast non-fat-suppressed (pre-NFS), and dynamic fat-suppressed (dyn-FS) images.

Results—When scores were averaged over readers, Dixon-RAVE achieved significantly higher ($p < 0.001$) degree of fat suppression compared to VIBE, for both pre-FS (4.25 vs. 3.67) and dyn-FS (4.10 vs. 3.46) images. Although Dixon-RAVE had lower IQ score compared to VIBE for the pre-FS (3.56 vs. 3.67, $p = 0.490$), the pre-NFS (3.54 vs. 3.88, $p = 0.009$), and the dyn-FS images (3.06 vs. 3.67, $p < 0.001$), acceptable or better diagnostic quality was achieved (score ≥ 3). The FG score for Dixon-RAVE in comparison to VIBE was significantly higher for the pre-FS image (4.23

Corresponding author: Thomas Benkert, Ph.D., New York University School of Medicine, Center for Biomedical Imaging, 660 First Avenue, 2nd floor, New York, NY 10016, Phone: 646-754-8016, Fax: 212-263-7541, thomas.benkert@nyumc.org.

vs. 3.85, p = 0.044), lower for the pre-NFS image (3.98 vs. 4.25, p = 0.054), and higher for the dynamic fat-suppressed image (3.90 vs. 3.85, p = 0.845).

Conclusions—Dixon-RAVE can serve as one-stop-shop approach for comprehensive T1-weighted breast MRI with diagnostic image quality, high spatiotemporal resolution, reduced overall scan time, and improved fat suppression compared to conventional imaging.

Keywords

breast MRI; DCE-MRI; dynamic contrast enhanced imaging; comprehensive imaging; fat/water separation; Dixon imaging; compressed sensing; parallel imaging; radial sampling; Dixon-RAVE

INTRODUCTION

Dynamic contrast-enhanced (DCE-) MRI is an important tool for diagnosis of breast cancer with superior sensitivity compared to mammography, ultrasound, and clinical breast exam.[1] For reliable assessment of tumor morphology and contrast kinetics, ideally both high spatial and high temporal resolution are required. Because these are competing requirements with conventional sequences, T1-weighted fat-suppressed gradient-echo scans are usually optimized for high spatial resolution.[2] Consequently, the achievable temporal resolution is often only in the order of 1–3 minutes, giving limited access to the kinetic characteristics of contrast enhancement.

To overcome this problem, several techniques have been proposed that enable DCE breast imaging with high spatiotemporal resolution, including golden-angle radial sparse parallel (GRASP)[3–5] and time-resolved angiography with stochastic trajectories (TWIST)[6,7]. However, like conventional Cartesian T1-weighted acquisitions, these methods rely on fat suppression, which can be inhomogeneous across the field-of-view and possibly obscure pathologies. Furthermore, a separate pre-contrast T1-weighted non-fat-suppressed acquisition is usually needed to assess fat-containing lesions, which further prolongs the overall scan time.

Dixon fat/water separation is a well-established technique that allows improving the robustness and uniformity of fat suppression in various applications,[8–10] including DCE breast MRI with TWIST.[11–13] However, using a TWIST-type approach can introduce errors in the signal-intensity time course due to the use of a view-shared reconstruction.[13,14] An alternative approach is the recently described Dixon-RAVE (radial volumetric encoding) method,[15] which combines radial sampling, fat/water separation, compressed sensing, and parallel imaging to achieve DCE imaging with robust fat suppression and high spatial as well as high temporal resolution. Besides contrast-enhanced images, pre-contrast fat-suppressed and non-fat-suppressed images can be extracted from the same dataset, thus enabling comprehensive T1-weighted DCE-MRI with reduced overall scan time.

The purpose of this study was to evaluate the clinical applicability of Dixon-RAVE as one-stop-shop approach for DCE breast imaging and to compare the results obtained with conventional clinical T1-weighted non-fat-suppressed and fat-suppressed images.

MATERIALS AND METHODS

Patient Population

This Health Insurance Portability and Accountability Act (HIPAA)-compliant prospective study was performed with approval from our Institutional Review Board (IRB) and waived informed consent. From March 2016 to October 2016, 24 consecutive patients (age 51.2±14.9 years; range 30–82 years) underwent diagnostic bilateral breast DCE-MRI examination on a clinical 3T scanner (Magnetom Tim Trio, Siemens Healthineers, Erlangen, Germany), which was equipped with a 16-channel breast coil array. Six (25%) of the patients were newly diagnosed with breast cancer and underwent the breast MRI for local pre-operative staging. The remaining 18 (75%) patients were asymptomatic high risk women who underwent screening breast MRI.

Data Acquisition

For the Dixon-RAVE method, data were acquired continuously with a prototypical T1-weighted gradient-echo sequence that uses a golden-angle stack-of-stars trajectory. In each repetition time, three echoes were sampled with a blipped bipolar readout.[15] The proposed Dixon-RAVE acquisition was added to the routine breast protocol as follows. Before injection of contrast agent, both a non-fat-suppressed and a fat-suppressed T1-weighted Cartesian VIBE scan were performed as part of the conventional protocol. Then, the Dixon-RAVE scan was performed with 400 radial projections, continuously acquired for 3:10 min. After the first 2 min of the Dixon-RAVE scan, a single dose of gadobutrol (Gadavist; Bayer Healthcare LLC, Whippany, NJ) at 0.1 mM/kg body weight was injected at a rate of 2 mL/s using an intravenous catheter and followed by a saline flush. The scan continued for the remaining 1:10 min. It was immediately followed by the acquisition of four conventional fat-suppressed Cartesian VIBE images. With this modified protocol, the initial phase of contrast uptake was captured with Dixon-RAVE, while the VIBE scans covered the phases that were required for routine clinical reading. The entire procedure is schematically depicted in Figure 1a. The combined acquisition time for the pre-contrast fat-suppressed, the pre-contrast non-fat-suppressed, and one contrast-enhanced VIBE scan was 6:33 min, while the acquisition time for Dixon-RAVE was 3:10 min.

Imaging parameters are shown in Table 1. For both the non-fat-suppressed and the fat-suppressed VIBE acquisitions, the scan parameters were chosen according to the conventional routine protocol at our institution. The image matrix size of Dixon-RAVE (320×320) was selected to achieve a high temporal resolution of 6.1 s/frame. Because the T1 weighting in gradient-echo acquisitions depends both on the repetition time and the flip angle, a higher flip angle, calculated using the Ernst angle equation[16], was chosen for Dixon-RAVE to account for the increased repetition time.

Image Reconstruction

All conventional VIBE scans were reconstructed on the scanner with the vendor-provided techniques. For the Dixon-RAVE datasets, two separate reconstructions were performed, which are schematically shown in Figure 1b.

1) To obtain static pre-contrast Dixon-RAVE water and fat images, only the first 260 projections were used, which were acquired before injection of the contrast agent. Retrospective selection of reconstruction windows is possible due to the golden-angle ordering scheme, which guarantees approximately uniform k-space coverage for any number of consecutively acquired projections.[17] For image reconstruction, the following optimization problem was iteratively solved:

$$\operatorname{argmin}\sum_{c,t}\|\mathrm{E}(W,F,\Phi)_{\mathrm{c,\,t}}-y_{\mathrm{c,\,t}}\|_2^2 \quad [1]$$

where y are the acquired 3D radial k-space data. The forward operator E transforms the to-be-estimated parameters, water (W), fat (F) and B_0 field map (Φ), to k-space data. Parallel imaging is incorporated by including precalculated coil sensitivity maps in the forward operator. Due to the moderate undersampling factor ($320 \cdot \pi/2/260 \approx 1.9$), the use of compressed sensing was omitted.

2) To generate dynamic image series, the entire dataset was used and 13 consecutive radial projections were combined into each dynamic frame. This results in a series of fat and water images with temporal resolution of 6.1 s per volume. Because the undersampling factor of the individual frames was $320 \cdot \pi/2/13 \approx 38.7$, compressed sensing was included in this case by solving the following optimization problem:

$$\operatorname{argmin}\sum_{c.t}\|\mathrm{E}(W,F,\Phi)_{\mathrm{c,\,t}}-y_{\mathrm{c,\,t}}\|_2^2+\lambda_{\mathrm{W}}\|\mathrm{S}(W)\|_1+\lambda_{\mathrm{F}}\|\mathrm{S}(F)\|_1+\lambda_{\Phi}\|\mathrm{S}(\Phi)\|_1 \quad [2]$$

Here, y are 4D k-space data (3 spatial and 1 temporal dimensions) and S are finite differences along the temporal dimension, which is equivalent to temporal total variation (TV) regularization.

Implementation Details

The forward operator E used in the above optimization problems (Equations 1 and 2) can be expressed as:

$$\mathrm{E}(W,F,\Phi)_{\mathrm{c,\,t}}=\mathrm{FT}\left(C_{\mathrm{c}}\cdot exp\left(2\pi\mathrm{i}\cdot\Phi\cdot t_n\right)\cdot W\right)+D\left(t\right)\cdot\mathrm{FT}\left(C_{\mathrm{c}}\cdot exp\left(2\pi\mathrm{i}\cdot\Phi\cdot t_n\right)\cdot F\right) \quad [3]$$

The operator FT performs a non-uniform fast Fourier transformation.[18] t_{n} are the different echo times and $D(t)$ is a sampling operator that models the chemical shift between water and fat in k-space. By using the exact readout time points of the samples for each spoke, the off-resonant blurring of fat, caused by the underlying radial trajectory, is corrected for.

The optimization problems were solved iteratively with a Gauss-Newton algorithm.[19] Convergence to the correct global minimum is not guaranteed due to the non-convexity of the problem. Therefore, a field map was precomputed as initialization step from all acquired data using a multi-seed safest-first region growing algorithm[20]. This field map was further

refined by inpainting (extrapolation or interpolation) of regions below a certain intensity-based threshold[21] and subsequent smoothing.

The image reconstruction was performed off-line because it requires the iterative computation of 3D datasets with many partitions. This was achieved by transferring the acquired data automatically to a dedicated reconstruction server using the Yarra software framework (https://yarra.rocks). Reconstruction was performed using in-house software written in Matlab R2015b (The Mathworks, Natick, MA). To reduce the computational complexity, readout oversampling was removed. Furthermore, a principal component analysis was used to compress the multi-channel dataset data into four eigenmodes.[22] After an inverse Fast Fourier Transform along the slice direction, individual slices were reconstructed simultaneously. Final results were exported in the DICOM format and sent to the picture archiving and communication system (PACS), from which they could be accessed for evaluation.

Reader Evaluation

Results were rated independently by two non-blinded board-certified radiologists (L.M., S.H.) with 15 and 7 years of experience. As indicated in Figure 1a, the following image sets were compared:

1. Pre-contrast non-fat-suppressed (pre-NFS) Dixon-RAVE image (generated synthetically by combining the extracted water and fat image) with pre-NFS VIBE image.
2. Pre-contrast water-only (pre-FS) Dixon-RAVE image with pre-contrast fat-suppressed (pre-FS) VIBE image.
3. Water-only image at the last time point of the dynamic Dixon-RAVE series with first post-contrast VIBE image, both referred to dyn-FS in the following.

A 5-point Likert-type scale (1 = poor, 5 = excellent) was used to rate the images in two categories, overall image quality (IQ) and conspicuity of fibroglandular tissue from fat (FG). Additionally, the degree of fat suppression (FS) was rated for the fat-suppressed images 1) and 3).

Statistical Analysis

Mean, median, standard deviation, and 25^{th} and 75^{th} percentiles were calculated for all rated categories for each sequence. This was performed for the scores from both readers independently as well as averaged over the readers. Wilcoxon signed rank tests were used for statistical evaluation with Matlab R2015b (The Mathworks, Natick, MA), defining statistical significance as $p < 0.05$. In addition, box plots were created which include the median as well as the first and third quartiles.

To assess reader agreement, linear weighted kappa coefficients were calculated for the ordinal outcomes of each rated category of each comparison using SPSS Statistics 23 (IBM, Armonk, NY). Kappa (κ) values less than zero were interpreted as poor agreement, $0 < \kappa \leq 0.2$ as slight agreement, $0.2 < \kappa \leq 0.4$ as fair agreement, $0.4 < \kappa \leq 0.6$ as moderate agreement, and $0.6 < \kappa \leq 0.8$ as substantial agreement.

RESULTS

Table 2 shows the scores from both readers independently. For each sequence, diagnostic quality (score > 3) was achieved for both readers in all categories. Reader agreement ranged from poor to fair agreement ($\kappa = -0.008 – 0.284$) for Dixon-RAVE and from poor to moderate agreement ($\kappa = -0.062 – 0.485$) for VIBE. When the scores from the different rated categories are pooled for each reader, readers had slight agreement for Dixon-RAVE ($\kappa = 0.162$) and fair agreement for VIBE ($\kappa = 0.335$) for the pre-FS images. For the pre-NFS images, slight reader agreement for both Dixon-RAVE ($\kappa = 0.176$) and VIBE ($\kappa = 0.029$) was achieved. Fair agreement for both sequences (Dixon-RAVE: $\kappa = 0.390$, VIBE: $\kappa = 0.288$) was obtained for the dyn-FS images.

Scores averaged over the two readers are shown in Table 3. When comparing the pre-FS images, the proposed method achieved significantly higher conspicuity of fibroglandular tissue from fat (4.23±0.51 vs. 3.85±0.52, $p = 0.0044$) and degree of fat suppression (4.25±0.44 vs. 3.67±0.64, $p < 0.001$) than the conventional VIBE technique. Although the reader agreement for the degree of fat suppression for Dixon-RAVE was poor, the p-values calculated for both readers independently also showed significantly better fat suppression with Dixon-RAVE (Table 2, $p < 0.001$ and $p = 0.033$, respectively). Image quality for Dixon-RAVE was lower than for VIBE (3.56±0.52 vs. 3.67±0.60, $p = 0.490$), although the difference was not significant.

For the pre-NFS images, Dixon-RAVE achieved significantly lower but still diagnostic image quality (3.54±0.41 vs. 3.88±0.34, $p = 0.009$) and lower conspicuity of fibroglandular tissue from fat (3.98±0.45 vs. 4.25±0.47, $p = 0.054$) compared to VIBE. This finding did not change when the p-values were calculated for both readers independently.

While image quality of the dyn-FS image was significantly lower with Dixon-RAVE compared to VIBE (3.06±0.34 vs. 3.67±0.60, $p < 0.001$), Dixon-RAVE achieved higher conspicuity of fibroglandular tissue from fat (3.90±0.39 vs. 3.85±0.56, $p = 0.0845$) and significantly higher degree of fat suppression (4.10±0.51 vs. 3.46±0.53, $p < 0.001$).

Figure 2 shows box plots of the averaged reader scores for each rated category for all three different image comparisons. Image quality was scored as diagnostic (3 and higher) in all cases except for two RAVE and one VIBE pre-FS cases, one pre-NFS RAVE scan and one dyn-FS RAVE scan.

Figure 3 shows different dynamic frames from the water image series, reconstructed from a representative Dixon-RAVE dataset. The achieved temporal resolution of 6.1 s per volume enables clear depiction of the contrast inflow, revealing marked background parenchymal enhancement.

Figure 4 and 5 show results for two patients with breast cancer using the conventional protocol (first row) and the proposed comprehensive Dixon-RAVE approach (second row).

DISCUSSION

Uniform suppression of fat signal is challenging in breast MRI due to B0 inhomogeneity caused by the complex anatomy and variation in tissue types across the FOV. Dixon methods improve the robustness of fat removal in the presence of B0 inhomogeneity.[23] Dixon-RAVE has been proposed as fast imaging method that enables dynamic contrast-enhanced 3D MR imaging with high spatiotemporal resolution and simultaneous fat/water separation. The underlying Dixon technique allows generating not only fat-suppressed water images but also water-suppressed fat images, as commonly acquired to assess fat-containing lesions. Hence, all clinically required T1-weighted contrasts are obtained within a single acquisition. In this study, the use of Dixon-RAVE as one-stop-shop approach for comprehensive T1-weighted breast imaging was evaluated in a clinical setting.

The underlying radial k-space sampling scheme allows for high acceleration factors with only mild streaking artifacts. In comparison to conventional Cartesian sampling, several additional technical challenges exist. To avoid artifacts caused by system imperfections such as gradient delays, the k-space shift along the readout direction needs to be estimated by acquiring additional projections before the actual image acquisition.[24] Another problem consists in the different appearance of chemical-shift effects. Because fat components are shifted along the readout direction, artifacts appear as unidirectional translation with conventional Cartesian sampling. Due to the varying readout direction for radial sampling, the effect results in blurring of the fat components, which was accounted for in the Dixon-RAVE approach by including the effect into the signal model. A further difference between the radial sampling scheme of Dixon-RAVE compared to the Cartesian sampling scheme of the conventional method is the appearance of artifacts. While motion can lead to ghosting artifacts in Cartesian acquisitions, radial acquisitions show lower sensitivity to motion and artifacts appear as more benign streaks.[25] Another origin of streaking is undersampling of k-space, which could be observed for some patients.

For all shown dynamic Dixon-RAVE results, 13 projections per frame were chosen, which corresponds to an undersampling factor of 38.7. This results in a temporal resolution of 6.1 s per volume, which enables capturing the fast signal enhancement in arterial vessels and malignant lesions.[4] By using a Fibonacci number (e.g., 8, 13, 21, 34, 55, and so forth) for the number of consecutive projections per frame, near-uniform k-space coverage of the different frames could be guaranteed.[17]

While most undersampling artifacts are removed by the iterative reconstruction process, residual streaking could be seen in some subjects. One way to overcome these artifacts is to reduce the undersampling factor by using more projections per frame. Due to the golden-angle reordering, this can be done retrospectively without changing the acquisition scheme. Combining more projections per frame, of course, reduces the temporal resolution. In the current implementation of Dixon-RAVE, three echoes were acquired for each repetition time. While the use of a bipolar readout allows performing this in a time-efficient way, the repetition time and, thus, the achievable temporal resolution can be further reduced by using two-point techniques[26].

In the present study, Dixon-RAVE was compared with conventional fat-suppressed and non-fat-suppressed VIBE scans. It should be noted, however, that several other approaches exist that also enable fat/water-separated DCE breast imaging with high spatial and high temporal resolution. One example is Dixon-TWIST[11,12], which combines view sharing and two-point Dixon imaging. By additionally using CAIPIRINHA sampling, a temporal resolution of 11.9 s was achieved with CAIPIRINHA-Dixon-TWIST-VIBE for isotropic spatial resolution of 1 mm.[13] A similar approach is DIfferential Subsampling with Cartesian Ordering (DISCO), which is likewise based on view sharing, 2-point Dixon fat/water separation, and parallel imaging. DISCO enables DCE breast MRI with spatial resolution of 0.8×0.8×1.6 mm^3 and temporal resolution of 27 s[27]. As in the present study, all these techniques were compared to conventional standard-of-care imaging techniques. However, to assess the performance of the different techniques with respect to each other, a comprehensive comparison would be required.

Our study has several limitations. Only 24 patients were recruited, and a higher number of subjects would be required to investigate the clinical utility for evaluation of lesions and the assessment of changes in clinical outcome. However, purpose of this initial study was to compare the overall image quality of Dixon-RAVE to conventional VIBE imaging. A prospective study in a larger patient population is planned to answer these remaining questions.

Due to the design of the imaging protocol, only the initial uptake of contrast agent was captured by the Dixon-RAVE scan. The last image of the reconstructed time series was compared to the first image of the subsequent VIBE acquisitions. Therefore, these images were acquired at slightly different time points after contrast injection. However, because the criteria for image-quality evaluation did not include the degree of contrast enhancement, a potential bias caused by the slightly different temporal offset is considered to be insignificant. As further limitation, the setup used here for evaluation of Dixon-RAVE did not allow assessment of the delayed phase of contrast enhancement. To allow for a more comprehensive comparison between Dixon-RAVE and the conventional protocol, two contrast injections during separate visits would be required for each patient. Another limitation consists in the use of different matrix sizes and, therefore, different spatial resolutions for the sequences. In accordance with the standard clinical in-house protocol, a matrix size of 448×358 and 448×291 was used for the non-fat-suppressed and the fat-suppressed VIBE scans, respectively. For Dixon-RAVE, a lower matrix size of 320×320 was used, which resulted in an in-plane resolution of 1.00×1.00 mm^2. The matrix size could be increased at expense of reduced temporal resolution.

Image reconstruction for the VIBE acquisitions was performed directly on the scanner and, therefore, results could be assessed by radiologists shortly after the scan. Dixon-RAVE, in contrast, requires solving an iterative optimization problem, which is computationally expensive. On a dedicated reconstruction server, the processing time for one dataset was ≈ 15–18 h. However, it is expected that the calculation time can be reduced significantly with a performance-optimized implementation in a low-level programming language or by using GPU computing.

In conclusion, this study demonstrates the potential utility of Dixon-RAVE as one-stop-shop approach for comprehensive T1-weighted DCE breast imaging. This is accomplished by using golden-angle radial sampling, model-based fat/water separation, parallel imaging, and compressed sensing. In comparison to conventional VIBE scans, Dixon-RAVE achieved lower, but still diagnostic image quality, higher temporal resolution, improved fat suppression, and overall reduced scan time.

Acknowledgments

The Center for Advanced Imaging Innovation and Research (CAI^{2}R, www.cai2r.net) at New York University School of Medicine is supported by NIH/NIBIB grant number P41 EB017183. We further acknowledge support by NIH grants 5R01EB018308 and 4R01CA160620.

References

1. DeMartini W, Lehman C. A review of current evidence-based clinical applications for breast magnetic resonance imaging. Top Magn Reson Imaging. 2008; 19(3):143–150. [PubMed: 18941394]
2. Kuhl CK, Schild HH, Morakkabati N. Dynamic bilateral contrast-enhanced MR imaging of the breast: trade-off between spatial and temporal resolution. Radiology. 2005; 236(3):789–800. [PubMed: 16118161]
3. Feng L, Grimm R, Block KT, et al. Golden-angle radial sparse parallel MRI: Combination of compressed sensing, parallel imaging, and golden-angle radial sampling for fast and flexible dynamic volumetric MRI. Magn Reson Med. 2014; 72(3):707–717. [PubMed: 24142845]
4. Kim SG, Feng L, Grimm R, et al. Influence of temporal regularization and radial undersampling factor on compressed sensing reconstruction in dynamic contrast enhanced MRI of the breast. J Magn Reson Imaging. 2016; 43(1):261–269. [PubMed: 26032976]
5. Heacock L, Gao Y, Heller SL, et al. Comparison of conventional DCE-MRI and a novel golden-angle radial multicoil compressed sensing method for the evaluation of breast lesion conspicuity. J Magn Reson Imaging. 2016; doi: 10.1002/jmri.25530
6. Tudorica LA, Oh KY, Roy N, et al. A feasible high spatiotemporal resolution breast DCE-MRI protocol for clinical settings. Magn Reson Med. 2012; 30(9):1257–1267.
7. Mann RM, Mus RD, van Zelst J, et al. A novel approach to contrast-enhanced breast magnetic resonance imaging for screening. Invest Radiol. 2014; 49(9):579–585. [PubMed: 24691143]
8. Clauser P, Pinker K, Helbich TH, et al. Fat saturation in dynamic breast MRI at 3 Tesla: is the Dixon technique superior to spectral fat saturation? A visual grading characteristics study. Eur Radiol. 2014; 24:2213–2219. [PubMed: 24792515]
9. Michaely HJ, Attenberger UI, Dietrich O, et al. Feasibility of gadofosveset-enhanced steady-state magnetic resonance angiography of the peripheral vessels at 3 Tesla with dixon fat saturation. Invest Radiol. 2008; 43:635–641. [PubMed: 18708857]
10. Haneder S, Koziel K, Morelli JN, et al. Clinical application of 3D VIBECAIPI-DIXON for non-enhanced imaging of the pancreas compared to a standard 2D fat-saturated FLASH. Clin Imaging. 2014; 38:142–147. [PubMed: 24332974]
11. Le Y, Kroeker R, Kipfer HD, et al. Development and evaluation of TWIST Dixon for dynamic contrast-enhanced (DCE) MRI with improved acquisition efficiency and fat suppression. J Magn Reson Imaging. 2012; 36(2):483–491. [PubMed: 22544731]
12. Le Y, Kipfer H, Majidi S, et al. Application of time-resolved angiography with stochastic trajectories (TWIST)-Dixon in dynamic contrast-enhanced (DCE) breast MRI. J Magn Reson Imaging. 2013; 38(5):1033–1042. [PubMed: 24038452]
13. Hao W, Zhao B, Wang G, et al. Influence of scan duration on the estimation of pharmacokinetic parameters for breast lesions: a study based on CAIPIRINHA-Dixon-TWIST-VIBE technique. Eur Radiol. 2015; 25(4):1162–1171. [PubMed: 25323603]

14. Song T, Laine AF, Chen Q, et al. Optimal k -space sampling for dynamic contrast-enhanced MRI with an application to MR renography. Magn Reson Med. 2009; 61:1242–1248. [PubMed: 19230014]
15. Benkert T, Feng L, Sodickson DK, et al. Free-breathing volumetric fat/water separation by combining radial sampling, compressed sensing, and parallel imaging. Magn Reson Med. 2016; doi: 10.1002/mrm.26392
16. Ernst RR, Anderson WA. Application of Fourier Transform Spectroscopy to Magnetic Resonance. Revi Sci Instrum. 2004; 37:93–102.
17. Winkelmann S, Schaeffter T, Koehler T, et al. An optimal radial profile order based on the golden ratio for time-resolved MRI. IEEE Trans Med Imaging. 2007; 26(1):68–76. [PubMed: 17243585]
18. Fessler JA, Sutton BP. Nonuniform fast Fourier transforms using min-max interpolation. IEEE Trans Signal Process. 2003; 51(2):560–574.
19. Doneva M, Börnert P, Eggers H, et al. Compressed sensing for chemical shift-based water-fat separation. Magn Reson Med. 2010; 64(6):1749–1759. [PubMed: 20859998]
20. Berglund J, Johansson L, Ahlström H, et al. Three-point Dixon method enables whole-body water and fat imaging of obese subjects. Magn Reson Med. 2010; 63(6):1659–1668. [PubMed: 20512869]
21. Anderson AG, Pipe JG. Off-Resonance Map Extrapolation Using Image Inpainting. Proceedings of the 24th Annual Meeting of ISMRM, Singapore. 2016:4268.
22. Buehrer M, Pruessmann KP, Boesiger P, et al. Array compression for MRI with large coil arrays. Magn Reson Med. 2007; 57(6):1131–1139. [PubMed: 17534913]
23. Glover GH, Schneider E. Three-point dixon technique for true water/fat decomposition with B0 inhomogeneity correction. Magn Reson Med. 1991; 18(2):371–383. [PubMed: 2046518]
24. Block KT, Uecker M. Simple method for adaptive gradient-delay compensation in radial MRI. Proceedings of the 19th Annual Meeting of ISMRM, Montreal, Canada. 2011:2816.
25. Block KT, Chandarana H, Milla S, et al. Towards routine clinical use of radial stack-of-stars 3D gradient-echo sequences for reducing motion sensitivity. J Korean Soc Magn Reson Med. 2014; 18(2):87–106.
26. Eggers H, Börnert P. Chemical shift encoding-based water-fat separation methods. J Magn Reson Imaging. 2014; 40(2):251–268. [PubMed: 24446249]
27. Morrison CK, Henze Bancroft LC, DeMartini WB, et al. Novel high spatiotemporal resolution versus standard-of-care dynamic contrast-enhanced breast MRI. Invest Radiol. 2016; doi: 10.1097/RLI.0000000000000329

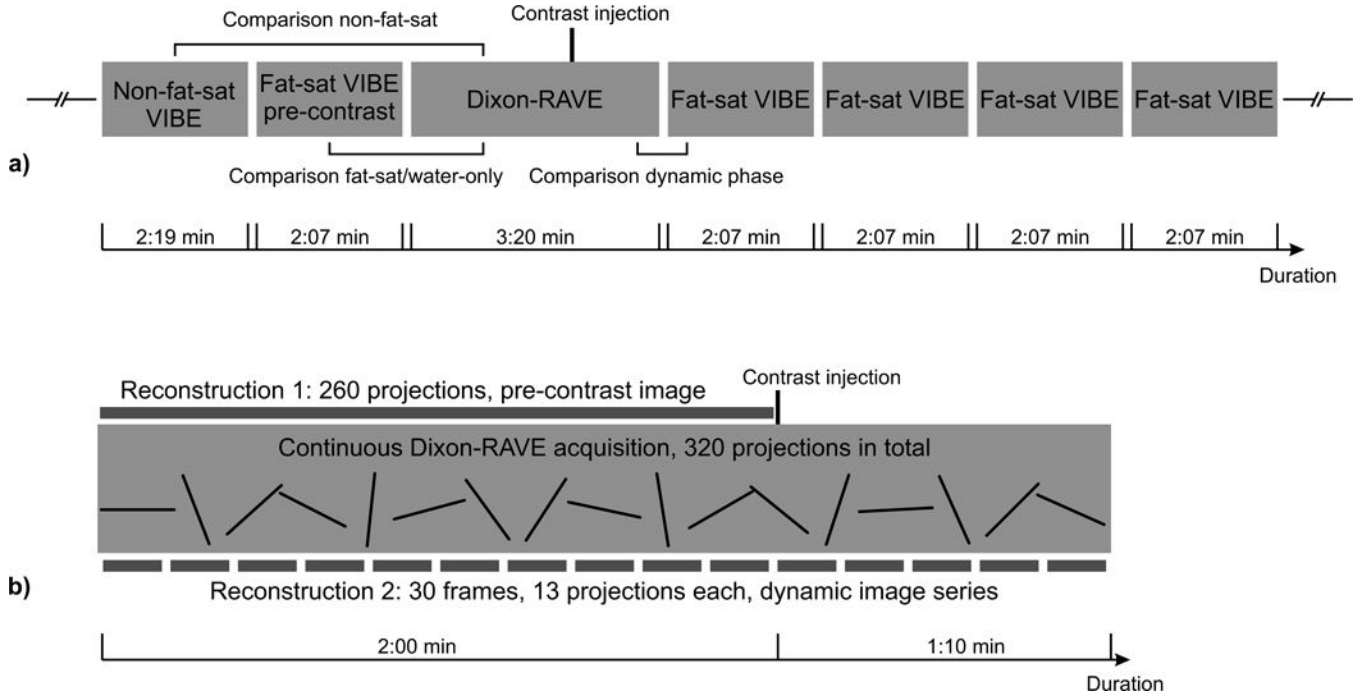

Figure 1.

a) Schematic illustration of the performed protocol, showing the different scans that were performed for each patient. Brackets indicate the comparisons that were used for the reader evaluation.

b) Overview of the two different Dixon-RAVE reconstructions. Reconstruction 1: To obtain static pre-contrast fat and water images, the first 260 projections were used. Reconstruction 2: For the dynamic image series, 13 consecutive projections were combined for each frame.

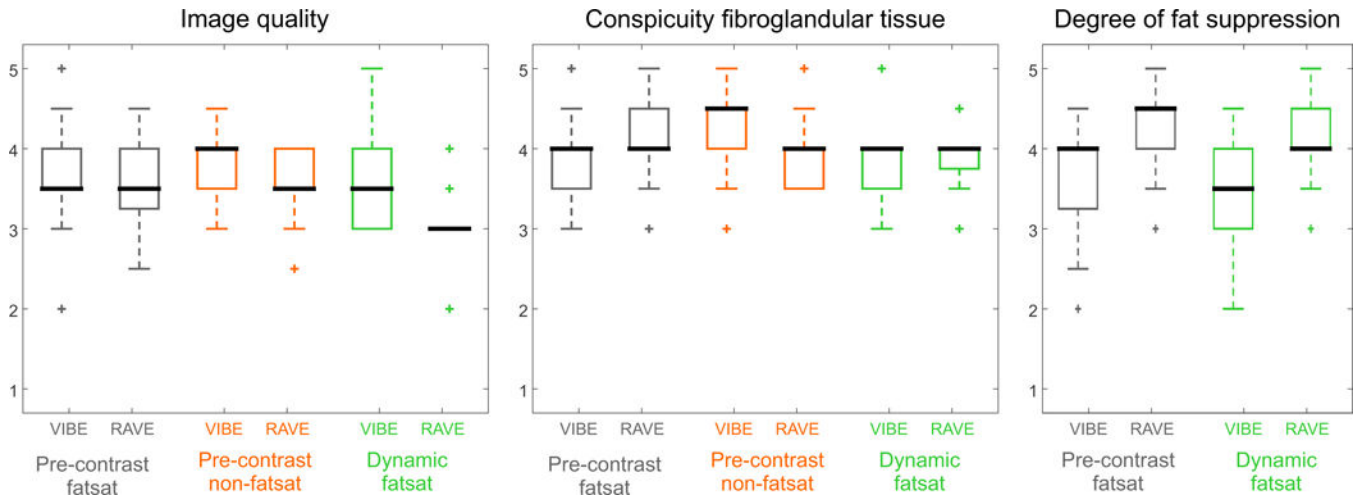

Figure 2.

Box plot for the scores for the different categories, averaged over both readers. The whiskers show 1.5 times the interquartile range.

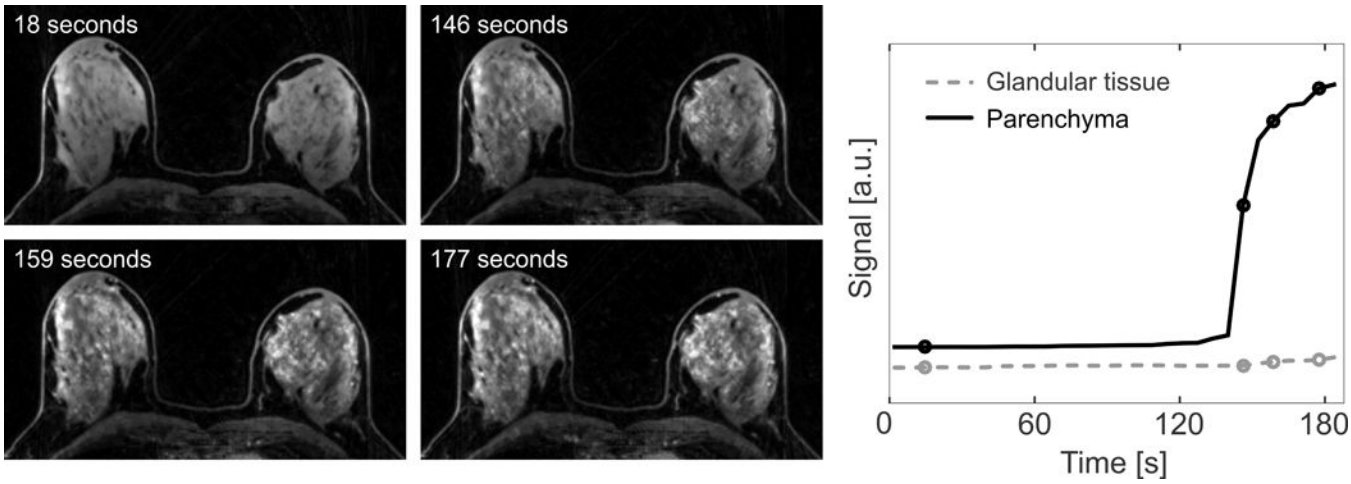

Figure 3.

Dynamic water series and extracted enhancement curves, generated from Dixon-RAVE. The temporal resolution of 6.1 s allows clearly showing the marked background parenchymal enhancement.

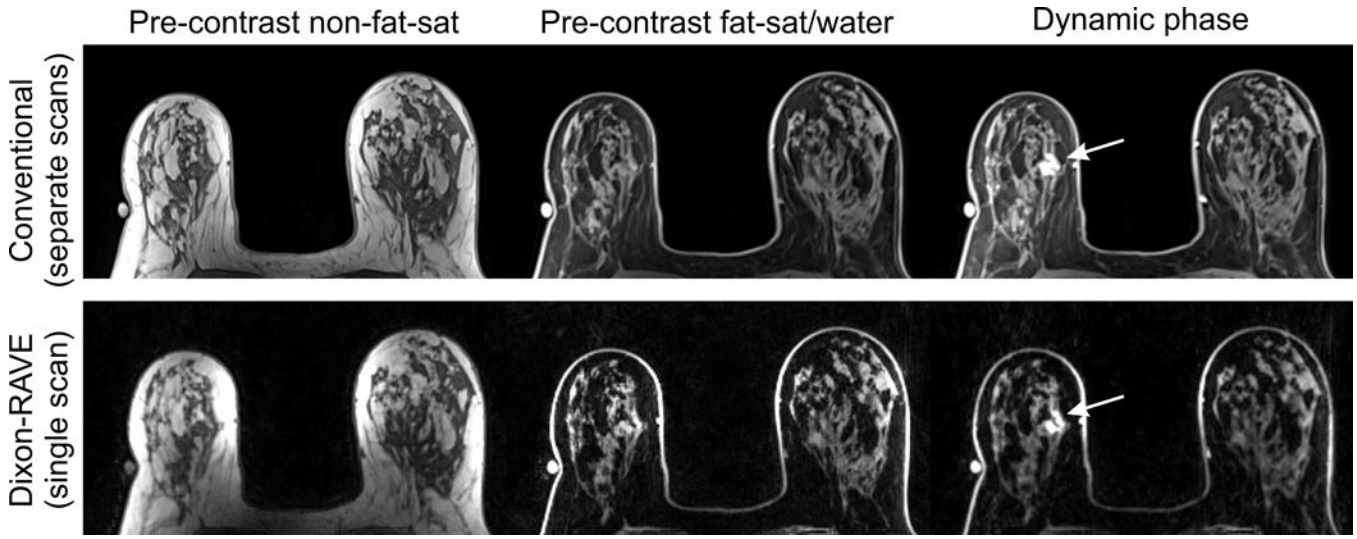

Figure 4.

Results for a 73-year-old patient with invasive lobular carcinoma (arrow) in the right breast. Dixon-RAVE achieves superior fat suppression compared to the conventional scans while maintaining diagnostic image quality.

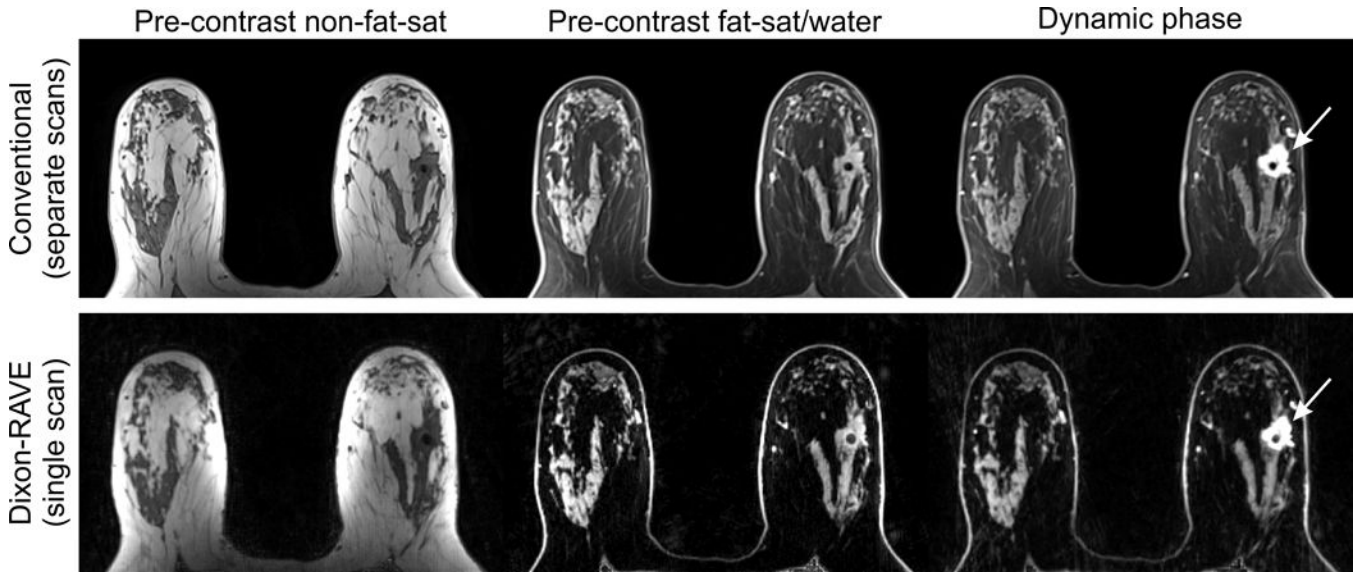

Figure 5.

Results for a 61-year-old woman with invasive ductal carcinoma (arrow). Similar diagnostic image quality and superior fat suppression is achieved with Dixon-RAVE compared to the conventional scans.

Table 1

Imaging parameters of the conventional VIBE and the proposed Dixon-RAVE protocols.

	Non-fat- suppressed VIBE	Fat- suppressed VIBE	Dixon-RAVE
Field of view	320×320 mm^2	320×320 mm^2	320×320 mm^2
Matrix size	448×358	448×291	320×320
Resolution	0.71×0.89 mm^2	0.71×1.10 mm^2	1.00×1.00 mm^2
Slice thickness	1.10 mm	1.10 mm	1.20 mm
Acquired partitions	192	192	144
Slice resolution	61%	61%	50%
Repetition time	4.74 ms	4.74 ms	6.54 ms
Echo time	1.79 ms	1.79 ms	1.50/3.12/4.74 ms
Flip angle	10°	10°	13°
Acquisition time	2:19 min	2:07 min	3:10 min

Table 2

Scores from both readers (1 = worst, 5 = best) for image quality (IQ), conspicuity of fibroglandular tissue from fat (FG), and degree of fat suppression (FS), expressed as mean ± standard deviation (first row) and median [25th percentile; 75th percentile] (second row).

Comparison 1: Pre-FS images

	Reader 1			Reader 2			κ	
	VIBE	**RAVE**	**p-value**	**VIBE**	**RAVE**	**p-value**	**VIBE**	**RAVE**
IQ	**3.67±0.64** 4 [3;4]	3.63±0.58 4 [3;4]	1.000	**3.67±0.76** 4 [3;4]	3.50±0.72 4 [3;4]	0.348	0.294	0.161
FG	3.88±0.54 4 [4;4]	**4.00±0.66** 4 [4;4]	0.432	3.83±0.64 4 [3;4]	**4.46±0.66** 5 [4;5]	0.011	0.485	0.284
FS	3.88±0.68 4 [4;4]	**4.58±0.58** 5 [4;5]	<0.001	3.46±0.83 4 [3;4]	**3.92±0.58** 4 [4;4]	0.033	0.250	−0.008

Comparison 2: Pre-NFS images

	Reader 1			Reader 2			κ	
	VIBE	**RAVE**	**p-value**	**VIBE**	**RAVE**	**p-value**	**VIBE**	**RAVE**
IQ	**3.88±0.34** 4 [4;4]	3.79±0.41 4 [4;4]	0.688	**3.88±0.54** 4 [4;4]	3.29±0.62 3 [3;4]	0.005	0.086	0.111
FG	**4.50±0.66** 5 [4;5]	4.21±0.51 4 [4;4.5]	0.092	**4.00±0.66** 4 [4;4]	3.75±0.61 4 [3;4]	0.241	−0.062	0.152

Comparison 3: Dyn-FS images

	Reader 1			Reader 2			κ	
	VIBE	**RAVE**	**p-value**	**VIBE**	**RAVE**	**p-value**	**VIBE**	**RAVE**
IQ	**3.83±0.64** 4 [3;4]	3.17±0.38 3 [3;3]	<0.001	**3.50±0.78** 3 [3;4]	2.96±0.55 3 [3;3]	0.011	0.371	0.160
FG	**4.08±0.65** 4 [4;4.5]	3.75±0.44 4 [3.5;4]	0.093	3.63±0.71 3.5 [3;4]	**4.04±0.62** 4 [4;4]	0.037	0.333	0.154
FS	3.75±0.53 4 [4;4]	**4.42±0.65** 4.5 [4;5]	<0.001	3.17±0.82 3 [3;4]	**3.79±0.51** 4 [3.5;4]	0.006	0.139	0.211

For each category, agreement between the two readers is expressed with the κ-values. Results are shown for all three performed comparisons. The technique with the higher score for each category is highlighted in bold. Statistical significant differences ($p < 0.05$) are underscored.

Table 3

Scores for the three comparisons (1 = worst, 5 = best), averaged over the two readers. p-values, mean ± standard deviation (first row), and median [25th percentile; 75th percentile] (second row) are shown for image quality (IQ), conspicuity of fibroglandular tissue from fat (FG), and degree of fat suppression (FS).

Comparison 1: Pre-FS images

	VIBE	RAVE	p-value
IQ	**3.67±0.60** 3.5 [3.5;4]	3.56±0.52 3.5 [3.25;4]	0.490
FG	3.85±0.52 4 [3.5;4]	**4.23±0.51** 4 [4;4.5]	0.044
FS	3.67±0.64 4 [3.25;4]	**4.25±0.44** 4.5 [4;4.5]	<0.001

Comparison 2: Pre-NFS images

	VIBE	RAVE	p-value
IQ	**3.88±0.34** 4 [3.5;4]	3.54±0.41 3.5 [3.5;4]	0.009
FG	**4.25±0.47** 4.5 [4;4.5]	3.98±0.45 4 [3.5;4]	0.054

Comparison 3: Dyn-FS images

	VIBE	RAVE	p-value
IQ	**3.67±0.60** 3.5 [3;4]	3.06±0.34 3 [3;3]	<0.001
FG	3.85±0.56 4 [3.5;4]	**3.90±0.39** 4 [3.75;4]	0.845
FS	3.46±0.53 4 [3;4]	**4.10±0.51** 4 [4;4.5]	<0.001

Statistical significant differences ($p < 0.05$) are underscored. The technique with the higher score in each category is highlighed in bold.